












Fission modes in ^{223}Ac and ^{227}Pa compound nuclei

S. Ramakrishna Reddy ^{1,*}, A. Pal,^{2,3} S. K. Duggi ¹, T. Santhosh,^{2,3} Pankaj Shah,⁴ Tanya Singh ^{2,3}, K. Prameela ¹,
V. V. Parkar ^{2,3}, N. N. Deshmukh ⁴, P. K. Rath,⁵ Ramandeep Gandhi ^{2,3}, S. Santra ^{2,3}, P. C. Rout,^{2,3} E. Prasad ⁶,
P. V. Madhusudhana Rao ¹ and S. Appannababu ^{1,†}

¹Department of Nuclear Physics, Andhra University, Visakhapatnam 530003, India

²Nuclear Physics Division, Bhabha Atomic Research Centre, Mumbai 400085, India

³Homi Bhabha National Institute, Anushaktinagar, Mumbai 400094, India

⁴School of Sciences/Engineering, PP Savani University, Surat 394125, India

⁵Centurion University of Technology and Management, Paralakhemundi, Odisha 756104, India

⁶Department of Physics, Central University of Kerala, Kasaragod 671316, India



(Received 15 April 2024; revised 24 May 2024; accepted 28 June 2024; published 24 July 2024)

Mass-energy distributions for fission fragments produced in the reactions $^{18}\text{O} + ^{205}\text{Tl}$, ^{209}Bi are studied around the Coulomb barrier energies populating ^{223}Ac and ^{227}Pa compound nuclei at excitation energies $E^* \approx 26\text{--}36$ MeV. The experimental results, showing small shoulders on either side, indicate the presence of asymmetric fission along with symmetric fission. We have estimated the contribution of asymmetric fission by fitting the experimental data with a Gaussian function composed of three components (one symmetric and two asymmetric). A small fraction of the asymmetric fission component is observed at all excitation energies. The experimental results are found to be in reasonable agreement with the GEF predictions. The asymmetric fission observed at high excitation energies can be explained by using multichance fission in the GEF calculations.

DOI: [10.1103/PhysRevC.110.014622](https://doi.org/10.1103/PhysRevC.110.014622)

I. INTRODUCTION

Extensive research on charge, mass, energy, and angular distributions of fragments from heavy-ion fusion-fission reactions have provided significant insights into the complex dynamics of the fission [1–11]. It is well established that the parameters such as the collision energy of the interacting nuclei, the characteristics of the colliding nuclei (shape degrees of freedom, size, and spin), the landscape of the potential energy surface (PES), the contact configuration of the nuclei in the PES, and the presence of shell closures in the compound nucleus (CN) as well as fragments influence the fusion-fission dynamics [7–9, 12, 13]. Mass yield distributions in fusion-fission processes induced by heavy ions usually peak at symmetry. This symmetric split is predominantly due to the high excitation energy, so that the nucleus behaves like a liquid drop [13]. The observed properties were hence well described within the framework of the liquid drop model (LDM). The mass asymmetric fission observed in the actinides as well as preactinides at low excitation energies, however, cannot be explained by the LDM [14–16]. The asymmetric fission observed in the neutron, proton, and photon-induced fission of reactions using uranium targets [17–19] was attributed to the fragment shell closures at $Z = 50$ and $N = 82$ in the heavy fragment and $N = 50$ in the lighter fragment [19].

The quantitative prescription by Strutinsky [20] provided a natural explanation of the observation of mass asymmetric fission in the actinide region. This prescription also explained the presence of fission isomers and allowed the estimation of microscopic shell effects on fission barriers in actinide nuclei. Furthermore, investigation of low-energy fission have shown the existence of different fission modes characterized by symmetric and asymmetric mass divisions. According to Brosa *et al.* [21], these modes, influenced by the shell structure of the fission fragments, corresponding to specific paths along the fission valleys of the PES, each with their own barrier and scission configurations. Thus, the first asymmetric mode, called standard I (S1) mode, is influenced by the doubly magic shell closure around ^{132}Sn , leading to a spherical heavy fragment and a compact scission configuration. The second and dominating asymmetric mode, referred as standard II (S2) mode, is characterized by a heavy fragment mass stabilized at $\langle A_H \rangle \approx 138\text{--}140$. Finally, a symmetric path leading to two highly deformed fission fragments defines the superlong (SL) mode. Early theoretical investigations suggested that the neutron shell closures at $N = 82$ and 88 (deformed neutron shell closure) in the heavy fragment were responsible for the existence of S1 and S2 modes of fission [22]. Recent experimental and theoretical studies show that the S2 mode is characterized by a heavy fragment stabilized around $Z = 54$ [19], which is related to a proton shell in octupole deformed fragments [23].

The recent observation of asymmetric fission in ^{180}Hg [24] triggered a new interest in fission of lighter nuclei. It was expected that shell effects would lead to a symmetric split in

*Contact author: ramakrishna.rs2020@gmail.com

†Contact author: appannababu@gmail.com

^{180}Hg , however, the data showed a distinct mass asymmetric fission, producing fission fragments with most probable masses of around $A_L = 80$ and $A_H = 100$. The asymmetric fission in $A \leq 200$ is significantly driven by the proton shell effect for $Z = 34\text{--}38$ in the light fragment and $Z = 44\text{--}46$ in the heavy fragment, according to microscopic models and an empirical analysis of the experimental data [8,23].

It is well established that the asymmetric mode observed in the low-energy fission of actinide nuclei transforms to symmetric mode with increasing excitation energy [1,13], due to damping of shell effects [25]. The triple-humped mass distribution corresponding to the symmetric and asymmetric modes observed in Radium nucleus is also seen to become symmetric at high excitation energy [26]. Even though the role of excitation energy on fission mass yield is known, the exact nature of the damping is yet not fully known.

It is interesting to note that the probability of successive neutron evaporation followed by multichance fission (MCF) increases with increasing excitation energy. Even if the excitation energy of the inhabited compound nucleus is substantially higher, the existence of MCF lowers the excitation energy of the remnant composite nuclei at every stage of chance fissions, resulting in the reappearance of a stronger shell effect. Several theoretical and experimental investigations address the role of MCF in the description of fission fragment mass distributions of actinide nuclei [27–31]. However, the scarcity of experimental data on the FF mass distribution for different compound nuclei over a range of excitation energies make it difficult to validate many of the theoretical predictions.

The objective of the present study is to investigate different possible modes of mass division in heavy-ion induced fission of ^{223}Ac and ^{227}Pa compound nuclei. We also aim to understand the role of MCFs in the measured mass distributions by comparing them with the predictions from the widely used semiempirical code GEF [19,30]. In the present work, we measured the fission fragment mass distributions (FFMD) for the reactions $^{18}\text{O} + ^{205}\text{Tl}$ and $^{18}\text{O} + ^{209}\text{Bi}$ around the Coulomb barrier energies in order to investigate the influence of shell closures and excitation energy dependence of symmetric and asymmetric mass divisions.

II. EXPERIMENTAL DETAILS

The experiment was performed at the Pelletron-LINAC facility Mumbai, India. A pulsed beam of ^{18}O with a repetition rate of 106.7 ns was bombarded on a self-supporting target of ^{209}Bi ($\approx 150 \mu\text{g}/\text{cm}^2$ thickness) and on an enriched target of ^{205}Tl ($\approx 190 \mu\text{g}/\text{cm}^2$ deposited on a $20 \mu\text{g}/\text{cm}^2$ carbon backing). Two position-sensitive multiwire proportional counters (MWPCs) with an active area of $12.5 \text{ cm} \times 7.5 \text{ cm}$ were used to detect the fission fragments in coincidence [32]. These MWPCs were kept at folding angle ($\theta_{\text{fold}} \approx 153^\circ$) at a distance of 30 cm from the target inside the scattering chamber, in order to detect the complementary fission fragments. The schematic diagram of the experimental setup is shown in Fig. 1. Two Si surface barrier detectors were placed at $\pm 15^\circ$ with respect to the beam direction at a distance of 70 cm from the target, in order to monitor the position of the beam on the target. The measurements were performed around the

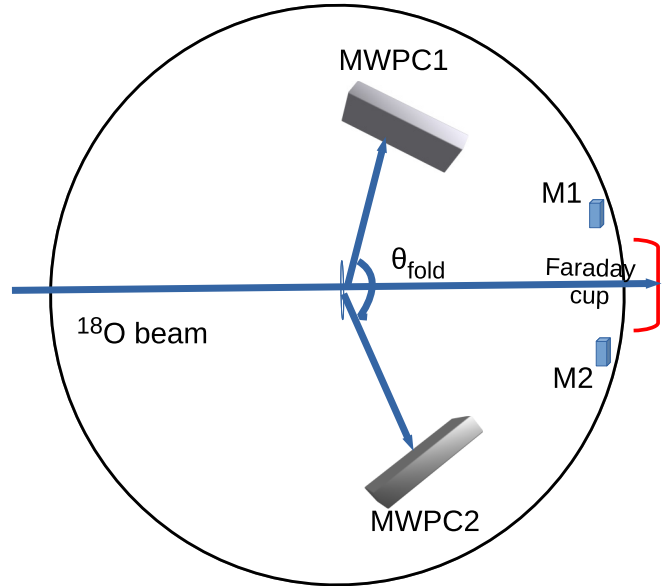


FIG. 1. A schematic diagram of the experimental setup used to measure the fission fragment mass yield distributions for $^{18}\text{O} + ^{205}\text{Tl}$, ^{209}Bi reactions.

Coulomb barrier energies ranging from 78 to 86 MeV in laboratory frame. The time of flight method was used to extract the FFMD. The timing correlation spectrum of the two MWPCs is shown in Fig. 2(a). The position calibration of the MWPCs are done by taking the reference of the edges of the detectors in online and off-line modes. In online mode, we have used the elastically scattered beamlike particles and fission data and in the off-line mode we have used ^{252}Cf source to determine the edges of the detectors. The calibrated X and Y position signals from both the detectors were converted into spherical-polar coordinates θ and ϕ event by event. To ensure the accurate timing measurements, a precision time calibrator is utilized, generating two signals, one serving as the START signal and the other as the STOP signal, with a suitable delay. By using the TOF, θ and ϕ information the velocities of the fragments were reconstructed. Using the kinematic reconstruction method, the time zero information was extracted by using the two conditions: (i) by ensuring that the parallel velocity

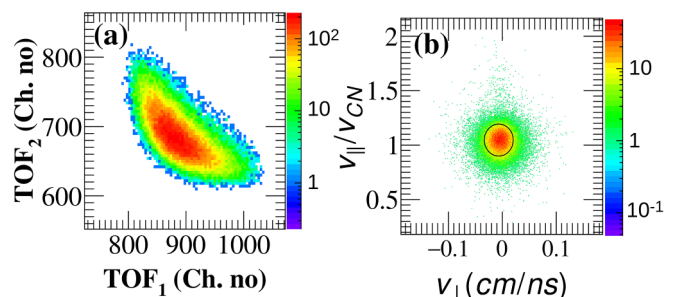


FIG. 2. (a) Time of flight spectra of MWPC1 versus MWPC2. (b) Measured distribution of velocity components of fission fragments for the reaction $^{18}\text{O} + ^{205}\text{Tl}$ ($E_{\text{lab}} = 86 \text{ MeV}$). Full momentum transfer fission events are shown inside the circle.

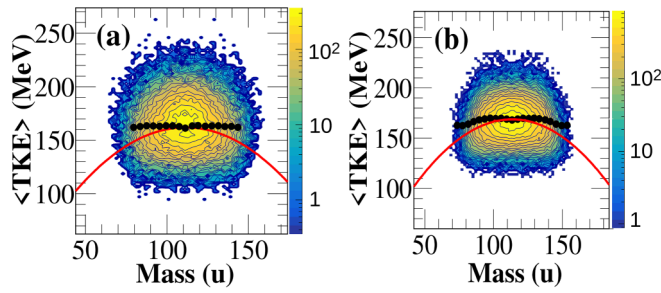


FIG. 3. The mass-TKE correlation plot for the reactions (a) $^{18}\text{O} + ^{205}\text{Tl}$ and (b) $^{18}\text{O} + ^{209}\text{Bi}$ at excitation energies 33.0 MeV and 31.5 MeV. The black solid circles represent the experimentally measured average total kinetic energies ($\langle \text{TKE} \rangle$) and the continuous line (red) represents the parabolic dependence as shown in Ref. [37].

component of the fissioning nucleus is equal to the velocity of the compound nucleus, and (ii) by observing a symmetric mass distribution obtained by calculating the ratio of fission fragment velocities ($v_{1c.m.}$, $v_{2c.m.}$) in the center-of-mass frame, centered around half of the compound-nucleus mass [33,34]. A typical two-dimensional (2D) plot for v_{\perp} versus $v_{\parallel}/v_{\text{CN}}$ is shown in Fig. 2(b), where both v_{\perp} and $v_{\parallel}/v_{\text{CN}}$ for the majority of the events are observed at 0 and 1, which corresponds to a complete fusion-fission events. The events inside the black circle in the Fig. 2(b) corresponding to the complete fusion-fission have been analyzed to extract the mass-total kinetic energy (TKE) distributions by using the two-body kinematics [35,36] event by event.

III. RESULTS AND DISCUSSION

Figure 3 shows the experimentally reconstructed mass-TKE correlation of the fission fragments for the reactions $^{18}\text{O} + ^{205}\text{Tl}$ and $^{18}\text{O} + ^{209}\text{Bi}$ at excitation energies 33.0 MeV and 31.5 MeV, respectively. The black solid circles represents the experimental $\langle \text{TKE} \rangle$ and the continuous line (red) represents the calculated $\langle \text{TKE} \rangle$ by using Viola systematics [37]. It may be observed that the measured $\langle \text{TKE} \rangle$ values for the symmetric mass division are in good agreement with the prediction of Viola systematics [37], whereas in the $\langle \text{TKE} \rangle$ of asymmetric split deviate significantly from the Viola systematics.

The 200% normalized FFMD for the CN ^{223}Ac and ^{227}Pa are shown in Fig. 4. The data show that the measured FFMD for the $^{18}\text{O} + ^{205}\text{Tl}$ reaction have small additional components on either side of the symmetric fission, while for the $^{18}\text{O} + ^{209}\text{Bi}$, the substantial components on either side of the main Gaussian for symmetric division. The experimental mass distribution is fitted using a sum of three Gaussian functions, one peaked at mass symmetry and other two on either side of the central Gaussian function. From the present analysis, it is found that for both the fissioning nuclei ^{223}Ac and ^{227}Pa , the mean position of the heavy fragment is peaked around $A_H = 136 \pm 1$ u, and is constant at all measured excitation energies. The mean mass of the lighter fragment is peaked at $A_L = 86 \pm 1$ u for ^{223}Ac and $A_L = 90 \pm 1$ u for ^{227}Pa . This observation is consistent with the previous reports [38], in which A_H remains

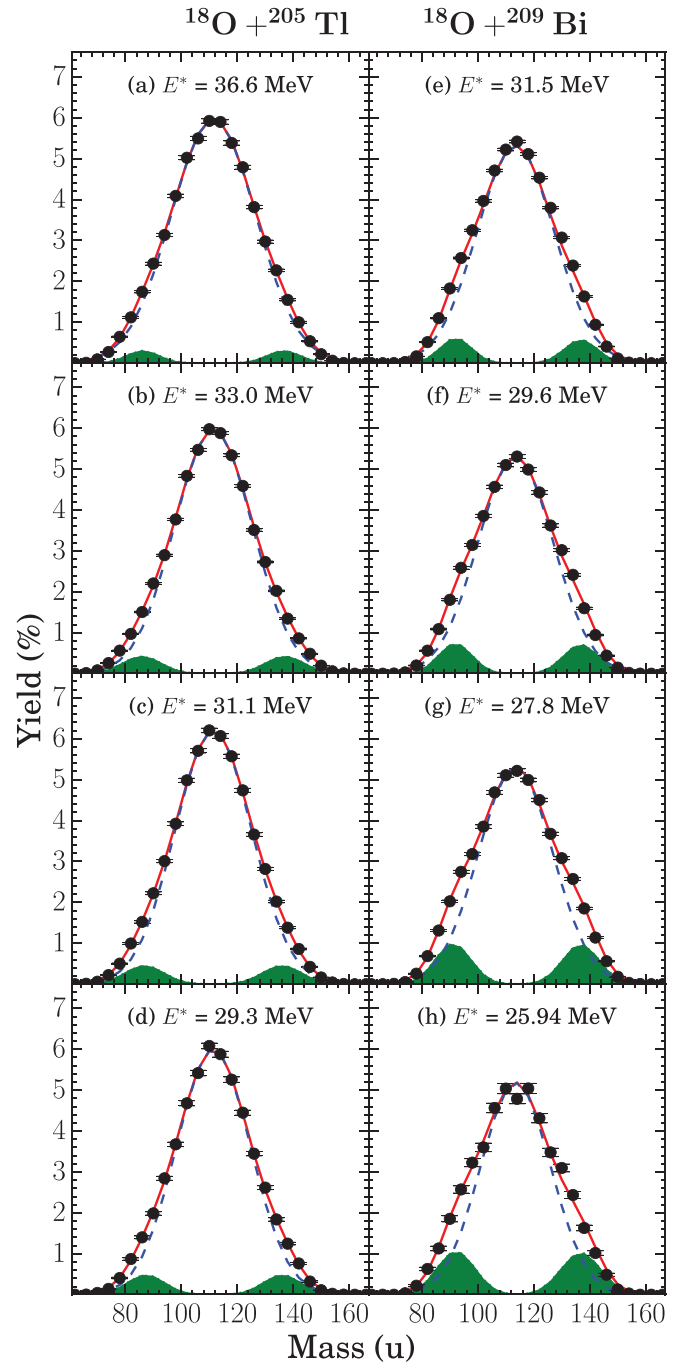


FIG. 4. The experimental mass distributions of fission fragments (solid circles) (a)–(d) for the reaction $^{18}\text{O} + ^{205}\text{Tl}$ and (e)–(h) for the $^{18}\text{O} + ^{209}\text{Bi}$ at different excitation energies. The lines correspond to the decomposition of mass distributions into the symmetric (blue dashed line), the asymmetric (green shaded), and total fission modes (red line).

fixed and it is independent of mass of the fissioning nucleus, while A_L increases with increasing mass of the fissioning nucleus. The presence of these asymmetric components with fixed peak positions for the heavy fragment, indicate the presence of shell effects in fission process even at an excitation energy of 36.6 MeV. The most probable neutron and proton numbers are estimated based on the unchanged charge

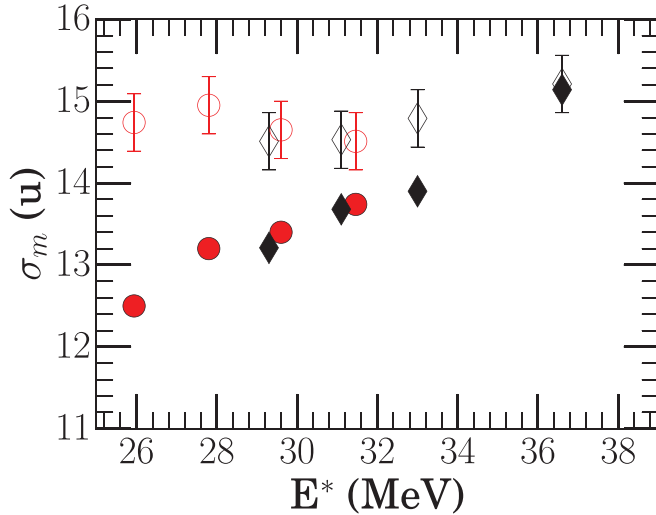


FIG. 5. The standard deviation in mass distribution, as a function of compound nucleus excitation energy, obtained from (i) overall experimental distributions (σ_m^{exp}) for the ^{223}Ac (open black diamonds) and ^{227}Pa (open red circles) and (ii) only the single Gaussian fit representing symmetric fission (σ_m^{sym}) for the ^{223}Ac (black diamonds) and ^{227}Pa (red circles).

distribution (UCD) assumption [16] for the heavy fragment corresponding to the asymmetric mode. It can be noted that the mean proton and neutron numbers for the heavy fragment are $Z_H \approx 54$ and $N_H \approx 82$, respectively. Our experimental results indicate the presence of the asymmetric component could be either due to the influence of a neutron shell closure at $N_H \approx 82$ or a deformed proton shell at $Z_H \approx 54$.

The experimentally obtained values of mass widths averaged over all fission modes σ_m^{exp} and the mass widths obtained for symmetric fission from the Gaussian fits σ_m^{sym} for ^{223}Ac and ^{227}Pa are shown in Fig. 5 as a function of excitation energy. One can observe that there is a large difference between the values of σ_m^{exp} and σ_m^{sym} . Moreover, mass widths are increasing with decreasing excitation energy, particularly at energies below the barrier. This indicates that shell effects are more dominant at lower excitation energies and are getting damped as the excitation energy increases.

The asymmetric yields [Y_A (%)] of the FFMD for the fissioning nuclei ^{223}Ac and ^{227}Pa as a function of excitation energy is shown in Fig. 6. It is found that the asymmetric yield for both reactions decreases with increasing excitation energy as expected. The asymmetric yield contribution for ^{223}Ac and ^{227}Pa at the lowest measured excitation energy are 7.4% and 18.1%, while at the highest measured excitation energy are 4% and 8.5%, respectively. The asymmetric yield is comparable at 31 MeV of excitation energy and follows a similar trend, consistent with the results of ^{227}Pa [39]. Also, it is observed that the asymmetric mode contribution is smaller for ^{223}Ac than ^{227}Pa , indicating that the possible effect of Z and N in the fissioning nuclei.

The semiempirical model code GEF [30] has been used to get further insights into the FFMD of ^{223}Ac and ^{227}Pa in order to understand the dependence of the excitation energy on competition between different modes of fission. GEF calculations

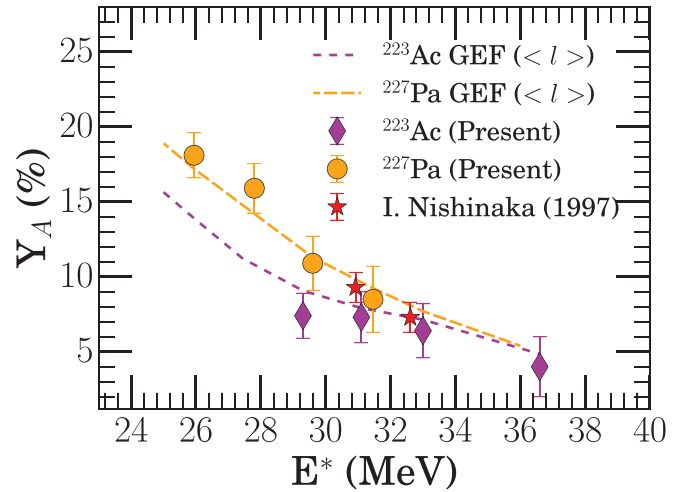


FIG. 6. The excitation energy dependence of the asymmetric fission contribution extracted from the present experimental mass distributions for ^{223}Ac and ^{227}Pa compared with the results from Nishinaka *et al.* [39] and GEF predictions.

were performed at different values of (E^* , $\langle \ell \rangle$) corresponding to the experimentally measured excitation energies for the present reactions, taking into account of the multichance fission in the compound nucleus decay. The values of average angular momenta are obtained by using coupled channel code CCFULL [40].

The experimental FFMDs are compared to the GEF predictions in Fig. 7. The predictions include the fission chance breakdown for ^{223}Ac and ^{227}Pa at $E^* \approx 31$ MeV.

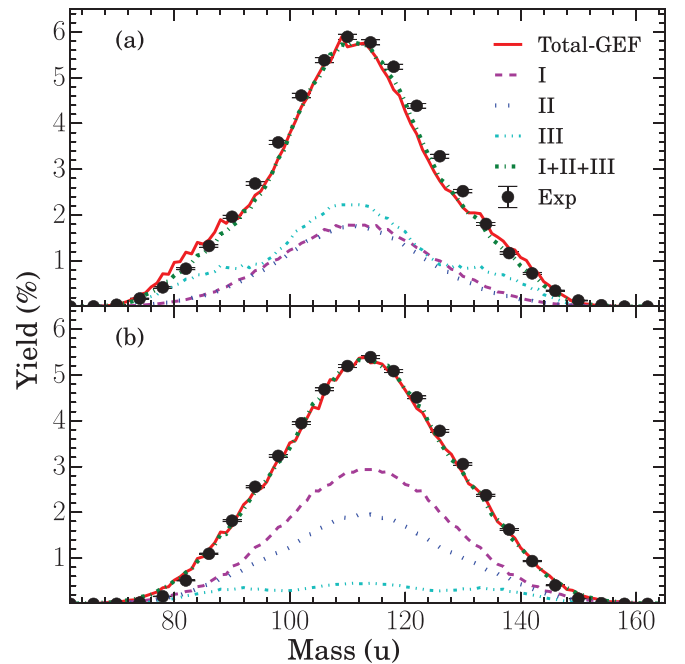


FIG. 7. Comparison of experimental FFMD for (a) ^{223}Ac and (b) ^{227}Pa at 31 MeV excitation energy along with the GEF calculations (including contributions from individual I, II, and III chance fission).

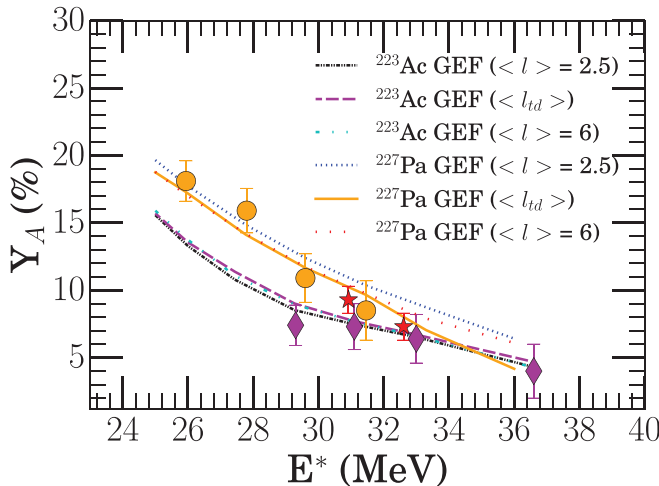


FIG. 8. The contribution of asymmetric fission as a function of excitation energy extracted from the present experimental mass distributions for ^{223}Ac (magenta diamonds) and ^{227}Pa (orange circles) compared with the results from Nishinaka *et al.* [39] (red stars) and GEF predictions using different angular momenta.

The calculated first and second chance mass distributions for ^{223}Ac are symmetric while that for the third chance has both symmetric and asymmetric components. For ^{227}Pa , the first and second chance appear symmetric, but with broader widths, while, again, the third chance has both symmetric and asymmetric components. One can observe from the Figs. 6 and 7 that the GEF predictions are in good agreement with the experimental data.

The weighted sum of mass distributions for each chance from the GEF calculations yields gross mass distributions very similar to the experimental data. To check for the sensitivity of the calculations to the mean angular momentum, calculations were performed with average spins of $\langle l \rangle = 2.5$, 6 and $\langle l_{td} \rangle$, the latter the average of the rolled over triangular fusion distribution calculated from PACE IV code [41] at different excitation energies. The contributions for symmetric and asymmetric components in the total mass distributions were calculated at each CN excitation energy by adding the weighted contributions from all three possible chances. The contribution of asymmetric fission as a function of excitation energy compared with the GEF predictions using different angular momenta was shown in Fig. 8. One observes that the contribution of the asymmetric fission mode increases with decreasing of $\langle l \rangle$, indicating that lower $\langle l \rangle$ values favors survival from fission, which may lead to the increase in the contribution of higher chance fission. Previously, it is also

reported that for a particular excitation energy the asymmetric fission contribution systematically decreases from lighter to heavier compound nuclei in this mass region, which may be due to the decrease in the fission barriers, leading to enhanced symmetric fission contributions [31].

IV. CONCLUSION

The fission fragment mass-TKE distributions were measured for the $^{18}\text{O} + ^{205}\text{Tl}$ and $^{18}\text{O} + ^{209}\text{Bi}$ reactions forming ^{223}Ac and ^{227}Pa compound nuclei around the Coulomb barrier energies. The mass-TKE correlations show evidence of the presence of asymmetric component, when the experimental $\langle \text{TKE} \rangle$ values are compared with the calculated values from the LDM. The mean mass of the heavy fragment of the asymmetric component is $A_H = 136 \pm 1$ for both systems. The mean mass of the light fragment increases with the mass on the fissioning system with $A_L = 86 \pm 1$ and $A_L = 90 \pm 1$ for the ^{223}Ac and ^{227}Pa compound nuclei, respectively. It shows that the mean mass of A_L is varying with the mass of the fissioning nucleus. According to the UCD model, 82 and 54 are the most likely N and Z values, respectively, for the heavy fragment that correspond to the asymmetric mode of the both compound nuclei. It appears that either a proton-deformed shell and/or a standard neutron shell closure in the heavy fragment is driving the asymmetric fission mode. Furthermore, the difference between values of σ_m^{exp} and σ_m^{sym} is decreasing with increasing excitation energy. We conclude that the fading of shell effects clearly seen in the FFMD for both systems. It is also evident that the measured Y_A (%) values for ^{223}Ac are slightly lower than those for ^{227}Pa at lower excitation energies. However, at higher excitation energies, these values appear to be similar. In order to describe the experimental observations, theoretical calculations using GEF code were performed. The present experimental results are in good agreement with the GEF model predictions. Further measurements on charge distributions in this mass region will be very useful to understand the role of competition between neutron/proton closed shells (either $N = 82$ or $Z = 54$) favoring the asymmetric fission.

ACKNOWLEDGMENTS

The authors thank the Pelletron-LINAC crew for their support and providing a quality beam. We also like to thank the target laboratory at TIFR for fabricating the targets. S.R.R. and S.A. acknowledge financial support from the University Grants Commission, Government of India. S.K.D. and K.P. thank the Department of Science and Technology, Ministry of Science and Technology, Government of India, for providing the financial support through the INSPIRE fellowship.

- [1] R. Dubey, P. Sugathan, A. Jhingan, G. Kaur, I. Mukul, G. Mohanto, D. Siwal, N. Saneesh, T. Banerjee, M. Thakur, R. Mahajan, N. Kumar, and M. B. Chatterjee, *Phys. Lett. B* **752**, 338 (2016).
 [2] R. Kumar, M. Maiti, A. Pal, S. Santra, P. Kaur, M. Sagwal, A. Singh, P. C. Rout, A. Baishya, R. Gandhi, and T. Santhosh, *Phys. Rev. C* **107**, 034614 (2023).

- [3] A. Pal, S. Santra, P. C. Rout, R. Gandhi, A. Baishya, T. Santhosh, R. Tripathi, and T. N. Nag, *Phys. Rev. C* **104**, L031602 (2021).
 [4] D. Paul, A. Sen, T. K. Ghosh, Md. M. Shaikh, K. Atreya, S. Kundu, K. Banerjee, C. Bhattacharya, S. Bhattacharya, J. K. Meena, D. C. Biswas, B. N. Joshi, N. Kumar, G. K. Prajapati, Y. K. Gupta, K. Mahata,

- K. Ramachandran, and S. Pal, *Phys. Rev. C* **102**, 054604 (2020).
- [5] S. Dhuri, K. Mahata, A. Shrivastava, K. Ramachandran, S. K. Pandit, V. Kumar, V. V. Parkar, P. C. Rout, A. Kumar, A. Chavan, S. Kaur, and T. Santhosh, *Phys. Rev. C* **106**, 014616 (2022).
- [6] T. Banerjee, E. M. Kozulin, N. T. Burtebayev, K. B. Gikal, G. N. Knyazheva, I. M. Itkis, K. V. Novikov, T. N. Kvochkina, Y. S. Mukhamejanov, and A. N. Pan, *Phys. Rev. C* **105**, 044614 (2022).
- [7] K. Nishio, A. N. Andreyev, R. Chapman, X. Derkx, C. E. Düllmann, L. Ghys, F. P. Heßberger, K. Hirose, H. Ikezoe, J. Khuyagbaatar, B. Kindler, B. Lommel, H. Makii, I. Nishinaka, T. Ohtsuki, S. D. Pain, R. Sagaidak, I. Tsekhanovich, M. Venhart, Y. Wakabayashi, and S. Yan, *Phys. Lett. B* **748**, 89 (2015).
- [8] K. Mahata, C. Schmitt, S. Gupta, A. Shrivastava, G. Scamps, and K.-H. Schmidt, *Phys. Lett. B* **825**, 136859 (2022).
- [9] E. Prasad, D. J. Hinde, M. Dasgupta, D. Y. Jeung, A. C. Berriman, B. M. A. Swinton-Bland, C. Simenel, E. C. Simpson, R. Bernard, E. Williams, K. J. Cook, D. C. Rafferty, C. Sengupta, J. F. Smith, K. Vo-Phuoc, and J. Walshe, *Phys. Lett. B* **811**, 135941 (2020).
- [10] V. Kumar, K. Mahata, S. Dhuri, A. Shrivastava, K. Ramachandran, S. Pandit, V. V. Parkar, A. Chavan, A. Kumar, S. Kaur, and P. C. Rout, *Phys. Rev. C* **109**, 014613 (2024).
- [11] S. Gupta, K. Mahata, A. Shrivastava, K. Ramachandran, S. K. Pandit, P. C. Rout, V. V. Parkar, R. Tripathi, A. Kumar, B. K. Nayak, E. T. Mirgule, A. Saxena, S. Kailas, A. Jhingan, A. K. Nasirov, G. A. Yuldasheva, P. N. Nadtochy, and C. Schmitt, *Phys. Lett. B* **803**, 135297 (2020).
- [12] B. M. A. Swinton-Bland, M. A. Stoyer, A. C. Berriman, D. J. Hinde, C. Simenel, J. Buete, T. Tanaka, K. Banerjee, L. T. Bezzina, I. P. Carter, K. J. Cook, M. Dasgupta, D. Y. Jeung, C. Sengupta, E. C. Simpson, and K. Vo-Phuoc, *Phys. Rev. C* **102**, 054611 (2020).
- [13] A. Ya. Rusanov, M. G. Itkis, N. A. Kondratiev, V. V. Pashkevich, I. V. Pokrovsky, V. S. Salamatin, and G. G. Chubarian, *Phys. At. Nucl.* **71**, 956 (2008).
- [14] N. Bohr and J. A. Wheeler, *Phys. Rev.* **56**, 426 (1939).
- [15] L. Meitner, *Nature (London)* **165**, 561 (1950).
- [16] R. Vandenbosch and J. R. Huizenga, *Nuclear Fission* (Academic Press, New York, 1973).
- [17] C. Straede, C. Budtz-Jørgensen, and H.-H. Knitter, *Nucl. Phys. A* **462**, 85 (1987).
- [18] R. L. Ferguson, F. Plasil, F. Pleasonton, S. C. Burnett, and H. W. Schmitt, *Phys. Rev. C* **7**, 2510 (1973).
- [19] K.-H. Schmidt, S. Steinhauser, C. Bockstiegel, A. Grewe, A. Heinz, A. R. Junghans, J. Benlliure, H.-G. Clerc, M. de Jong, J. Muller, M. Pfutzner, and B. Voss, *Nucl. Phys. A* **665**, 221 (2000).
- [20] V. M. Strutinsky, *Nucl. Phys. A* **95**, 420 (1967).
- [21] U. Brosa, S. Grossmann, and A. Müller, *Phys. Rep.* **197**, 167 (1990).
- [22] B. D. Wilkins, E. P. Steinberg, and R. R. Chasman, *Phys. Rev. C* **14**, 1832 (1976).
- [23] G. Scamps and C. Simenel, *Nature (London)* **564**, 382 (2018).
- [24] A. N. Andreyev, J. Elseviers, M. Huysse, P. Van Duppen, S. Antalic, A. Barzakh, N. Bree, T. E. Cocolios, V. F. Comas, J. Diriken, D. Fedorov, V. Fedosseev, S. Franchoo, J. A. Heredia, O. Ivanov, U. Köster, B. A. Marsh, K. Nishio, R. D. Page, N. Patronis, M. Seliverstov *et al.*, *Phys. Rev. Lett.* **105**, 252502 (2010).
- [25] K. Hirose, K. Nishio, S. Tanaka, R. Leguillon, H. Makii, I. Nishinaka, R. Orlandi, K. Tsukada, J. Smallcombe, M. J. Vermeulen, S. Chiba, Y. Aritomo, T. Ohtsuki, K. Nakano, S. Araki, Y. Watanabe, R. Tatsuzawa, N. Takaki, N. Tamura, S. Goto *et al.*, *Phys. Rev. Lett.* **119**, 222501 (2017).
- [26] D. G. Perry and A. W. Fairhall, *Phys. Rev. C* **4**, 977 (1971).
- [27] P. Möller and C. Schmitt, *Eur. Phys. J. A* **53**, 7 (2017).
- [28] H. Paşca, A. Andreev, G. Adamian, and N. Antonenko, *Eur. Phys. J. A* **54**, 104 (2018).
- [29] S. Tanaka, Y. Aritomo, Y. Miyamoto, K. Hirose, and K. Nishio, *Phys. Rev. C* **100**, 064605 (2019).
- [30] K.-H. Schmidt, B. Jurado, C. Amouroux, and C. Schmitt, *Nucl. Data Sheets* **131**, 107 (2016).
- [31] S. Santra, A. Pal, D. Chattopadhyay, A. Kundu, P. C. Rout, R. Gandhi, A. Baishya, T. Santhosh, K. Ramachandran, R. Tripathi, B. J. Roy, T. N. Nag, G. Mohanto, S. De, B. K. Nayak, and S. Kailas, *Phys. Rev. C* **107**, L061601 (2023).
- [32] A. Pal, S. Santra, A. Kundu, D. Chattopadhyay, A. Jhingan, B. Nayak, and S. Prafulla, *J. Instrum.* **15**, P02008 (2020).
- [33] R. Rafiei, R. G. Thomas, D. J. Hinde, M. Dasgupta, C. R. Morton, L. R. Gasques, M. L. Brown, and M. D. Rodriguez, *Phys. Rev. C* **77**, 024606 (2008).
- [34] R. G. Thomas, D. J. Hinde, D. Duniec, F. Zenke, M. Dasgupta, M. L. Brown, M. Evers, L. R. Gasques, M. D. Rodriguez, and A. Diaz-Torres, *Phys. Rev. C* **77**, 034610 (2008).
- [35] D. J. Hinde, M. Dasgupta, J. R. Leigh, J. C. Mein, C. R. Morton, J. O. Newton, and H. Timmers, *Phys. Rev. C* **53**, 1290 (1996).
- [36] D. C. Biswas, R. P. Vind, N. Kumar, Y. K. Gupta, R. V. Jangale, A. L. Inkar, L. A. Kinage, B. N. Joshi, S. Mukhopadhyay, G. K. Prajapati, and S. Dubey, *Nucl. Instrum. Meth. Phys. Res. A* **901**, 76 (2018).
- [37] V. E. Viola, K. Kwiatkowski, and M. Walker, *Phys. Rev. C* **31**, 1550 (1985).
- [38] K. F. Flynn, E. P. Horwitz, C. A. A. Bloomquist, R. F. Barnes, R. K. Sjoblom, P. R. Fields, and L. E. Glendenin, *Phys. Rev. C* **5**, 1725 (1972).
- [39] I. Nishinaka, Y. Nagame, K. Tsukada, H. Ikezoe, K. Sueki, H. Nakahara, M. Tanikawa, and T. Ohtsuki, *Phys. Rev. C* **56**, 891 (1997).
- [40] K. Hagino, N. Rowley, and A. T. Kruppa, *Comput. Phys. Commun.* **123**, 143 (1999).
- [41] A. Gavron, *Phys. Rev. C* **21**, 230 (1980).